JOURNAL OF THERMOPHYSICS AND HEAT TRANSFER
Vol. 19, No. 4, October–December 2005

Transient Radiative Heat Transfer from a Plasma Produced by a Capillary Discharge

Malay Das,* Stefan T. Thynell,† Jianquan Li,* and Thomas A. Litzinger†
Pennsylvania State University, University Park, Pennsylvania 16802

The objective of this work is to develop a better understanding of the transient behavior of radiative heat transfer from a plasma. The plasma generation occurred within a 3.2-mm-diam and 26-mm-long polyethylene capillary. Because of its high temperature and high pressure, the plasma evolved from the capillary into an ambient air environment as an underexpanded supersonic jet that interacted with a stagnation plate. Various diagnostic techniques were used. They include heat flux and pressure gauges mounted on the stagnation plate, heat flux gauges and silicon photodiodes mounted below the plasma jet, as well as current transducers interfaced with the electrical circuit. The heat flux gauges were manufactured via sputtering and calibrated using a standard convection oven. A fused-silica window, placed about 1 mm above the gauges, ensured that only the radiative heat flux transmitted by the window was deduced. The row of heat flux gauges mounted below the plasma provided an assessment of the fraction of the radiative heat flux transmitted by the fused-silica window. The results show that the peak of emitted radiant flux occurs immediately after the peak of the discharge of electrical energy, which usually occurred a relatively long time prior to arrival of the precursor shock on the stagnation plate.

Nomenclature

c	=	specific heat, J/kg · K
k	=	conductivity, W/m · K
q''	=	heat flux, W/m^2
T	=	temperature, K
T_{ref}	=	ambient temperature, K
t	=	time, s
$V(t)$	=	voltage at time t, V
x	=	axial coordinate, m
α	=	thermal diffusivity, m^2/s
β	=	temperature coefficient of resistivity, 1/K
ρ	=	density, kg/m^3

I. Introduction

THE use of a high-temperature and high-pressure plasma for ignition of solid propellants has recently received considerable attention.[1–8] The high temperatures and pressures produce a complex interaction between the plasma and the propellant, involving several modes of energy transport. First, the characteristic velocities and thermal conductivity of the plasma are large, thereby producing high convective heat transfer coefficients. Second, the plasma contains electrons, ions, atoms, and low-molecular-weight species from the ablation of capillary and electrodes that contribute significantly to the thermal radiation in the UV/visible wavelength range. Third, as the plasma cools, particularly in the interaction region near the propellant's surface, heat is released from recombination reactions among electrons, ions, atoms, and low-molecular-weight species. Finally, chemical reactions between products from the solid propellant and products from the plasma may enhance the chemical reactions, thereby producing reduced ignition delays compared to conventional ignition systems. However, few studies are available in the literature that have attempted to characterize heat transfer rates from plasmas generated by capillary discharges.

Information about average heat flux rates to plasma-exposed surfaces were deduced by Williams and White.[9] They allowed plasma impingement on a black-carbon-coated thin copper plate. The temperature history on the back side of the plate was captured using an unfiltered infrared camera. An inverse analysis was utilized to deduce average heat flux rates from the temperature data. This work served as a refinement of the earlier effort by White et al.,[10] in which thermocouples were used on the back side of the copper plate. Infrared photography was utilized rather than thermocouples, because the electrical noise likely caused by rapidly varying electromagnetic fields was significant.

Taylor[11,12] performed radiative heat flux measurements on plasmas emerging from a long capillary into stagnant air at 1 atm. The experimental configuration was similar to the one used by Hankins and Mann[13] and Hankins et al.[14,15] A polyethylene capillary of about 175 mm in length was employed, coupled with very large input energy levels of 40 kJ. The copper initiation wire was 1 mm in diameter, which is significant. Time-resolved spectroscopy was utilized, covering the wavelength range from 258 to 892 nm. The spectrometer was calibrated using a standard deuterium lamp for wavelengths between 258 and 400 nm, and a tungsten lamp for 336 to 892 nm. Measurements at the exit port suggested that the radiant heat flux levels are much lower than expected, with maximum brightness temperatures of 14,500 K. In view of the deduced low radiant heat flux levels, Taylor[16] suggested that metal vapor condensation, with its concomitant release of latent heat, contributed significantly to the short ignition delays. In addition, Proud and Bourne[17] examined plasma injection after ignition of a nitroguanidine-based propellant; a 60% burn rate enhancement was observed but its cause was not explained.

In subsequent works, Taylor measured the radiative heat flux in plasma–propellant interactions using time-resolved UV/visible spectroscopy.[18,19] Measurements covered a wavelength range from 369 to 1027 nm, and spectra were acquired at a time resolution of about 50 μs. Experiments were conducted using two different configurations. Aluminum and copper wires of 0.5 mm diameter were used as plasma initiators. In the first case, the exploding wire was placed coaxially with an open-ended propellant cylinder. The second test case was conducted in a 400 cm^3 closed chamber by placing the propellant at one endplate and a capillary plasma generator at the opposite endplate. A conventional ignition system using a puffer bag was also tested in the second configuration. Using a translucent propellant, it was concluded that the damage sustained

Received 16 August 2004; revision received 3 January 2005; accepted for publication 6 January 2005.

*Research Assistant, Department of Mechanical and Nuclear Engineering. Member AIAA.

†Professor, Department of Mechanical and Nuclear Engineering. Senior Member AIAA.

in the propellant's internal grain structure was not attributed to the radiative heat flux. The type of material used for the plasma initiation wire played an important role in the damage of the propellant's grain structure.

Gruber et al.[20] and Kappen and Bauder[21,22] developed a model of spectral radiative heat transfer from high-temperature and high-pressure plasmas. Based on the assumption of local thermodynamic equilibrium, that is, translational, rotational, and vibrational temperatures are equal, the numerical framework can readily compute the radiation heat transfer with input of plasma properties, including temperature and partial pressure of a wide variety of ions, atoms, and diatomic and triatomic species. It appears that carefully conducted emission measurements from various hydrocarbon plasmas could yield important information about species present and line-of-sight temperatures at various positions using the developed code. For such an analysis, calibration of the acquired spectra is not needed. However, to deduce the total radiant heat flux, calibration is needed.

The preceding discussion reveals a limited understanding of the various heat transfer modes from capillary discharges. The objective of this study is twofold: 1) to describe a heat flux gauge design with a high-frequency response and 2) to quantify the transient variation of the radiative heat flux from a plasma produced by a capillary discharge.

II. Experimental Apparatus and Approach

A. Plasma Generator

A schematic of the electrical circuit and plasma chamber with gauge locations is shown in Fig. 1. The pulse-forming network (PFN) is mainly composed of an energy storage component that consists of two high-voltage, fast-discharge capacitors connected in parallel to yield a total capacitance of 192 μF, pulse-shaping components including a 20 μH inductor and a crowbar diode, a floating high-voltage mercury switch (ignitron), and a circuit for triggering the ignitron. The capacitors can be charged up to 10 kV to yield a maximum energy storage of 9.6 kJ. The plasma chamber consists of a capillary, a fine metallic wire, electrodes, and other nonconducting housing hardware. The capillary is made of high-density polyethylene, which is machined to have a bore length of 26 mm and a typical diameter of 3.2 mm. Located at each end of the capillary is an electrode made of elkonite (30% Cu, 70% W), which is resistant to material erosion. A fine copper wire of 0.16 mm diameter, which runs through the capillary and connects the electrodes, serves as the discharge initiator. After being formed immediately upon triggering the ignitron, the plasma flows through a nozzle that has dimensions of 3.2 mm (orifice diameter) and 26 mm (length) into the ambient open-air environment. The nozzle is designed to have this length simply for accommodating the relatively large dimensions of the plasma chamber, which is needed to maintain its structural integrity in case of anomalous pressure excursions.

Figure 2 shows the locations of the various gauges used in the experiment. Heat flux gauges are placed at two different locations. One location corresponds to measurements at the position of the pressure gauges on the stagnation plate, to yield the maximum heat

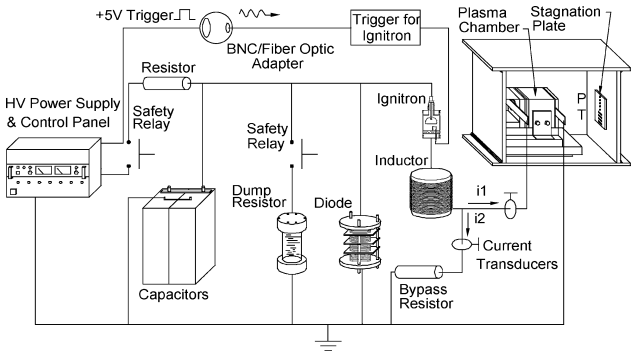

Fig. 1 Schematic of electrical circuit, plasma chamber, and location of stagnation plate.

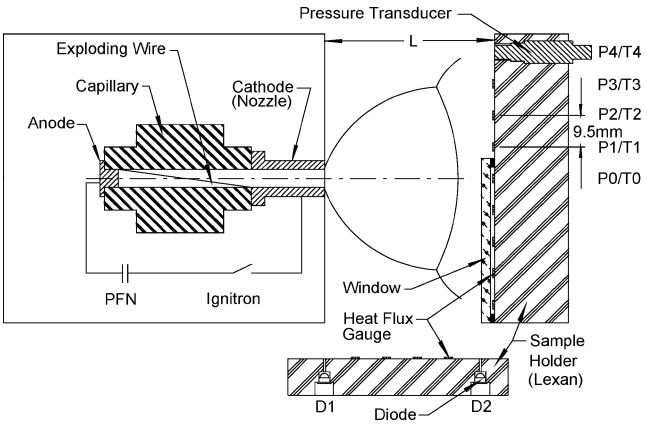

Fig. 2 Schematic of pressure transducer, heat flux gauge and diode locations with respect to plasma emergence from capillary.

flux rates. For this location, the gauges are covered with two fused-silica windows (S1-UV, ESCO Products): one sacrificial 1.59 mm thick and a second 4.76 mm thick. The second row of heat flux gauges is located below the plasma. It is used to determine the extent of transmission by the fused-silica window. The fused-silica window is needed for two reasons. First, the goal is to allow a determination of the radiative heat flux as opposed to the total heat flux (radiative, convective, and heat release from recombination reactions). The use of fused-silica windows allows the former but prevents the latter two energy-exchange mechanisms. Second, some ionic species or charged particles arrive at the plasma–solid interface and tend to produce significant electrical noise.

The diodes are used to determine plasma emergence (left diode) and plasma arrival (right diode). Diode 1 (Si) is located directly below the plasma exit port. Diode 2 is also located below the plasma flow, but is placed at a distance of 48 mm from diode 1. Both diodes thus have a side view of the plasma; their spectral range covers 300 to 900 nm. The diodes view the plasma through a 6-mm-long, 0.71-mm-diam hole and have a response time of <10 ns. The incident power on the diodes is thus reduced significantly.

Kistler pressure transducers were used (model 211B3) having a measurement range 0–34.47 bar. To avoid direct impact of the plasma on the transducers, the sensing areas of the pressure transducers were covered with a thin tape. Pearson coils are used to deduce the instantaneous current and voltage across the plasma. Data acquisition was performed at 1 MHz using 12-bit transient recorders (Nicolet MP120/150), whose minimum bandwidth is 400 kHz.

Side-view images of the plasma were taken using a Cordin model 222-B charge-coupled device (CCD) camera. It consists of 8 CCDs and is capable of acquiring 16 images, each with a resolution of 1300 by 1030 pixels, a 10-bit dynamic range, and exposure gates down to 10 ns. The first and last eight images can be acquired at a speed of up to 10^8 pictures per second, but these two sets of eight images are interrupted by a delay of several microseconds for transfer of the charge.

B. Heat Flux Gauge Design

A thin-film sensor and circuitry were designed and manufactured for deducing the transient variation of the radiative heat flux. The principle of its operation is that a constant current flows through a thin metal layer whose resistivity depends on temperature.[23–25] Once the surface temperature of the film is known from the calibrated resistance vs temperature relationship, an inverse technique is utilized to deduce the heat flux data corresponding to the temporal evolution of the measured surface temperature.[26–28] However, the thin-film gauge itself cannot isolate radiative flux from other heat transfer mechanisms. Either a large distance between the plasma source and the gauge or placement of transparent windows over the gauge can ensure measurement of radiative flux alone, preventing other modes of heat transfer. Issues related to design optimization of fast-response gauges have been discussed.[29]

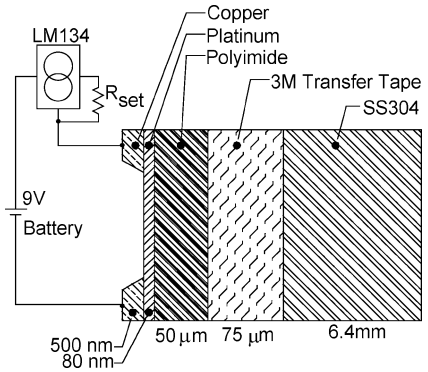

Fig. 3 Electrical circuit and layer design for platinum heat flux gauge.

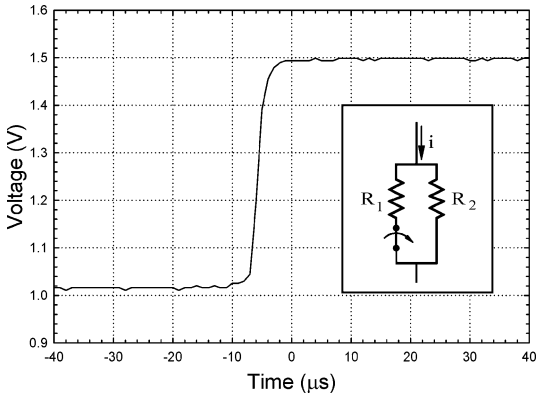

Fig. 4 Response of circuit containing LM 134 constant current source to a step increase in the resistance.

Figure 3 shows a cross-sectional view of the basic design of the thin-film heat flux gauge. The polyimide layer, which is 50 μm thick, has a low thermal conductivity (0.1 to 0.35 W/m · K) and is chemically stable for working temperatures up to 250 to 320°C.[‡] Sputtering of platinum at 0.67 Pa was employed to yield films that attach well to the polyimide substrate. The thickness of the sputtered platinum is typically 80 nm, and its width and length are, respectively, 0.25 and 12 mm. At each end of the platinum strip, 3-mm-wide copper leads of 500 nm thickness and 6 mm length were sputtered on top of the platinum. The electrical leads are soldered onto the copper lead to yield a high-strength and high-electrical-conductivity connection. A transfer tape is used to attach the polyimide film to the SS304 substrate. The constant current source is National Semiconductor's LM 134 chip, powered by a low-noise 9-V battery. The external resistor R_{sct} defines the current flowing through the gauge. The current is nominally set at 3 mA. This value produces insignificant self-heating of the gauge, while providing adequate protection to electrical noise produced early in the discharge process. Figure 4 shows the response of the electrical circuit to a step increase in the resistance; that is, the switch is suddenly opened. It is clear that the internal circuitry of the LM 134 constant current source responds quickly to the sudden change in resistance. Because the platinum film is thin and located on a poorly conducting substrate, the frequency response is high (>100 kHz), and it is controlled by the electrical circuit of the constant current source.

C. Data Reduction

A standard inverse approach was employed to estimate the transient, absorbed radiative heat flux variation from the measured time-dependent voltage data. The model assumes that conductive transfer in the polyimide film is one-dimensional, that a perfect thermal contact is made between the platinum film and the polyimide substrate, and that thermophysical properties are constant. The inverse problem is governed by

$$k\frac{\partial^2 T}{\partial x^2} = \rho c\frac{\partial T}{\partial t} \qquad 0 < x < \infty, \qquad 0 < t < t_f \tag{1}$$

$$-k\frac{\partial T}{\partial x} = q''(t) \qquad x = 0 \tag{2a}$$

$$T = T_{\text{ref}} \qquad x \to \infty \tag{2b}$$

$$T = T_{\text{ref}} \qquad t = 0 \tag{2c}$$

where $q''(t)$ is the unknown, absorbed radiative heat flux. Based on the conjugate-gradient approach described in detail by Ozisik,[28] a numerical procedure was developed. The inverse data reduction technique was applied to the measured surface temperature to determine the absorbed, radiative heat flux. The model used a thermal conductivity $k = 0.25$ W/m · K, which is the normal conductivity obtained by Kurabayashi et al.,[30] $\rho = 1420$ kg/m^3, and $c_p = 1040$ J/kg · K of the polyimide substrate. Because the width of the platinum is 250 μm and the polyimide thickness is 50 μm, the use of a one-dimensional film may raise concerns. It is possible to estimate the thermal wave penetration based on a uniform heat flux during a specified time interval. The analysis results in a thermal wave penetration depth $\delta \approx 2(\alpha \times t)^{1/2}$. With a maximum duration of about 300 μs of the plasma emission, the thermal wave penetration depth is approximately 14 μm. Hence, the use of a one-dimensional heat conduction model is very reasonable.

The temperature coefficient of the electrical resistivity of platinum, $\beta = 0.002$/K, was assumed to be linear over the temperature range from 20 to 220°C, and it was deduced from measurements using a standard convection oven. This value is about 50% lower than the bulk value (0.00389/K). For the manufactured film thickness of 80 nm, the incident radiant energy is either absorbed or reflected by the platinum film; the transmissivity is practically zero. The theoretical spectral absorptivity of platinum can be roughly estimated using bulk properties.[31] The diffuse or normal spectral absorptivity is about 0.75 at 200 nm, decreases to 0.4 at 400 nm, and about 0.32 at 600 nm. The platinum film appears slightly dark to the naked eye.

III. Discussion of Results

Figures 5 and 6 show eight images acquired by the Cordin 222-B CCD camera using an exposure time of 70 ns, with the first (top) image 40 μs after triggering and subsequent images separated by 20 μs. Images after 100 μs reveal a rapid decay of the plasma emission, with the eighth image showing only weak structures remaining of the plasma. The fourth image at $t = 100$ μs reveals that the gauge at the stagnation point (P0/T0) is covered by the plasma for all hemispherical solid angles. Plasma expansion, however, is significant, resulting in partial coverage for the outermost gauge position (P4/T4), which is located 38 mm from the stagnation point. Clearly, plasma emission is most significant in the region to the right of the Mach disk, which shows some curvature. General features of the underexpanded supersonic jet have been discussed elsewhere.[5,7,8,32]

Figures 7–9 show the results from open-air testing involving a distance between plasma exit port to stagnation plate of 50 and 75 mm, as well as charging voltages of 2.5, 3.0, and 4.0 kV. Figure 7 reveals that, irrespective of charging voltage, peak values of current i1 are reached at about 80 μs into the event. However, the duration of electrical energy conversion varies from about 190 to 220 μs. Current i1 represents the current flow through the plasma chamber. At the end of the i1 current flow, there is still some residual energy in the capacitor, however. It is slowly dissipated in the noninductive bypass resistor, which is used to deduce the instantaneous voltage drop across the plasma. The output from diode 1, shown in Fig. 8, reveals that the larger the charging voltage, the earlier the plasma emerges into the ambient air. This earlier plasma emergence is caused by increased rate of electrical energy conversion, producing a more rapid increase in pressures within the capillary and thus an earlier emergence of the plasma. For example, for a charging voltage of 4.0 kV, the plasma emerged 25 μs after triggering,

[‡]Data available online at http://www.goodfellow.com [cited 29 April 2005].

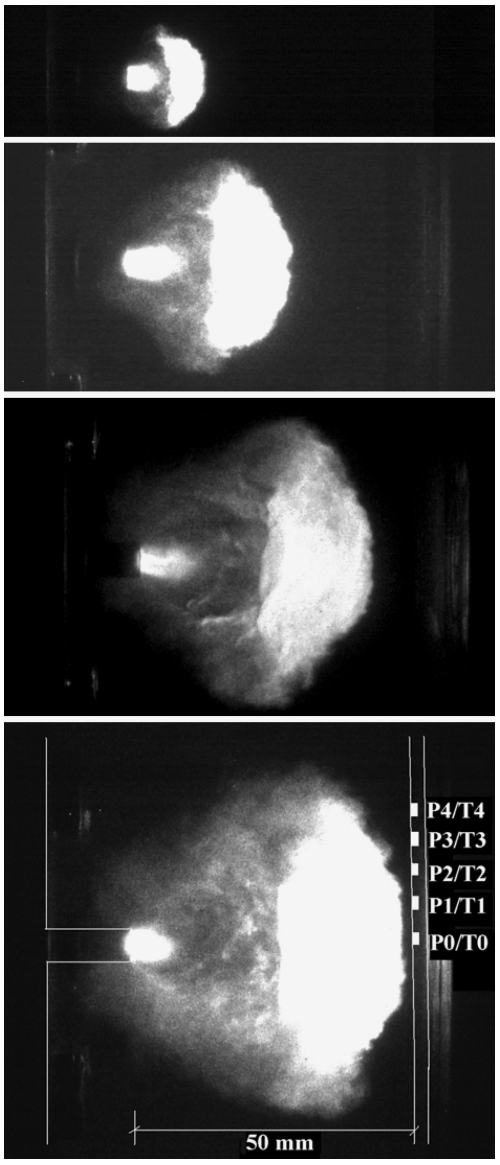

Fig. 5 Side-view images of plasma obtained from a charging level of 2.5 kV, and acquired 40 (top), 60, 80, and 100 μs (bottom) after triggering.

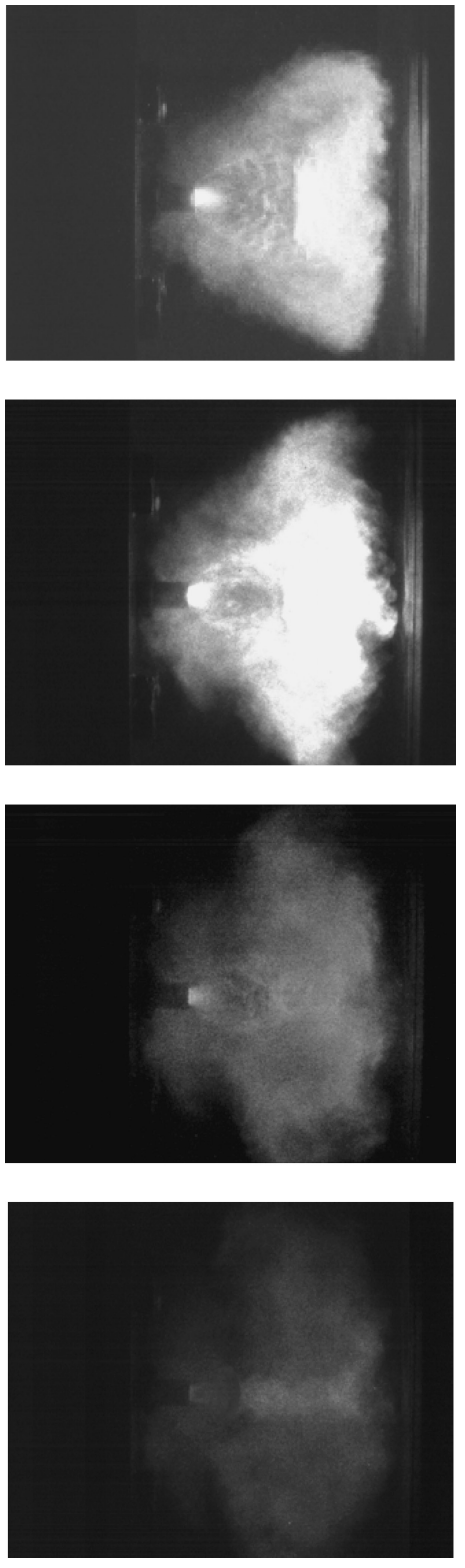

Fig. 6 Side-view images of plasma obtained from a charging level of 2.5 kV, and acquired 120 (top), 140, 160, and 180 μs (bottom) after triggering.

whereas the corresponding time was 32 μs for a charging level of 2.5 kV. Hence, times prior to plasma emergence are of little interest for both gasdynamic and heat transfer studies. The response of the second diode, shown in Fig. 9, also shows the plasma emergence at this early time, but this is caused by multiple reflections within the test facility. Diode 1, however, records peak radiant heat fluxes that are much larger than those of diode 2. The occurrence of the peak value of the heat flux of diode 1 is close to the occurrence of peak value of current i1. Diode 2 detects reemission in some tests after the completion of the electrical discharge ($t > 220$ μs). This reemission is probably due to interactions between plasma species and air, as well as recombination reactions among the plasma products. For small charging levels, the emission from the plasma is quite small. Diode 2 senses emission only from regions near the stagnation plate; because it very low compared to diode 1, the plasma has expanded and cooled significantly once reaching the stagnation plate.

The heat flux gauges were covered with two fused-silica windows (one is 1.59 mm thick, whereas the other is 4.76 mm thick); this window material is very pure and allows transmission over the wavelength range from about 170 to 2500 nm. The thin, sacrificial window is replaced after every test, because some slight degradation of the surface occurs. Additionally, only a small amount of sooty residue remains on the surface, in particular for the low charging level of 2.5 kV. The LM 134 constant current source is susceptible to interference from the rapidly changing electric and magnetic fields during the first 20 μs after triggering. Using a capacitor across the battery terminals has no effect. This interference is caused by two effects that produce high-frequency electric and magnetic fields. First, as the initiation wire is rapidly heated to its melting point, its electrical conductivity rapidly decreases as the wire expands due to thermal effects and breaks apart to form small droplets. Second, as

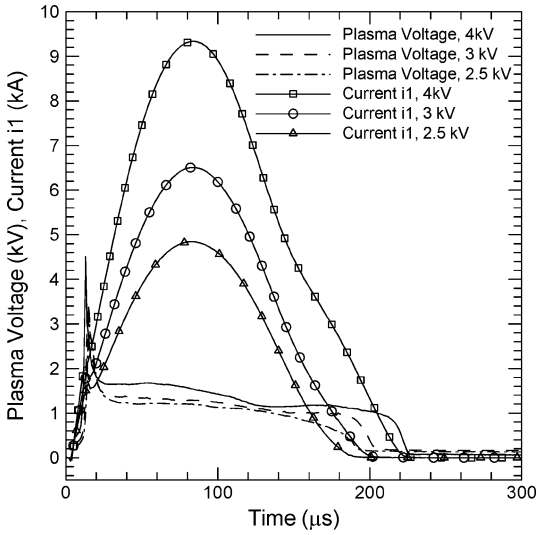

Fig. 7 Current and voltage drop in electrical circuit for a 3.2-mm-diam polyethylene capillary for charging voltages of 2.5 kV (0.6 kJ), 3.0 kV (0.86 kJ), and 4.0 kV (1.56 kJ).

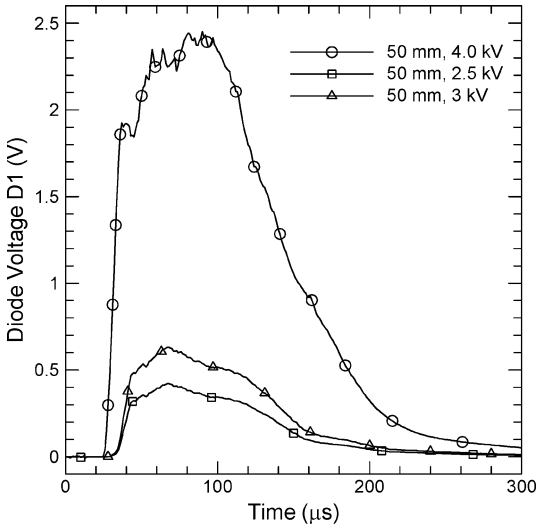

Fig. 8 Response of diode 1 due to emission from ablated products from polyethylene capillary, initiation wire, and nozzle for charging voltages of 2.5 kV (0.6 kJ), 3.0 kV (0.86 kJ), and 4.0 kV (1.56 kJ).

arcing occurs between the droplets, a highly conductive plasma is rapidly produced. During the plasma transitions from one containing metal ions and atoms to another containing carbon and hydrogen ions and atoms, as well as hydrocarbon ions and molecules, the electrical conductivity changes again. Once the plasma emerges from the capillary, a quasi-steady voltage is achieved until the electrical energy is nearly discharged.

Figures 10–13 show the pressure, gauge temperatures, and deduced absorbed radiant heat fluxes for charging levels of 2.5 and 3.0 kV, as well as distances between plasma chamber and stagnation plate of 50 and 75 mm; $T_{\text{ref}} = 20^{\circ}\text{C}$. The case shown in Fig. 10 yields the peak values: the film temperature rise is 160°C, the peak pressure is 8.8 bar, and the peak heat flux is 14.4 MW/m^2. Increasing the distance between plasma chamber and stagnation by 25 mm has a pronounced effect, as shown in Fig. 11. The peak film temperature is only 56°C and the heat flux reaches a peak of only about 3.8 MW/m^2. Increasing the charging level from 2.5 to 3 kV, shown in Fig. 12, yields a doubling in the peak heat flux, whereas the electrical energy stored in the capacitor is increased only by 44%. Examining the results for a gauge location of 9.5 mm above the stagnation point, shown in Fig. 13, reveals a 20% reduction in the peak heat flux. Hence the view factor between the plasma and gauge location

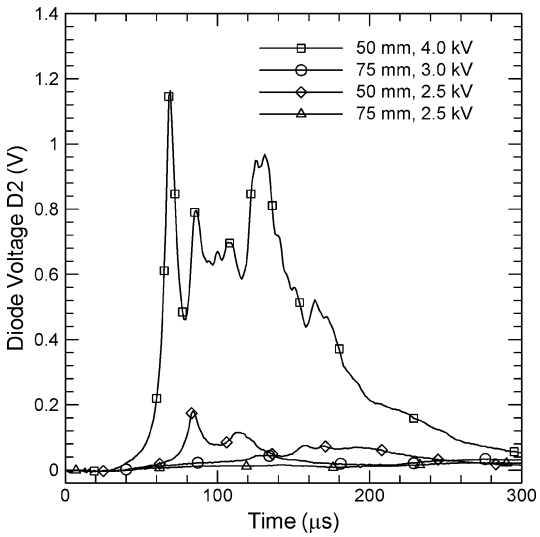

Fig. 9 Response of diode 2 due to emission from ablated products from polyethylene capillary, initiation wire and nozzle for charging voltages of 2.5 kV (0.6 kJ), 3.0 kV (0.86 kJ), and 4.0 kV (1.56 kJ).

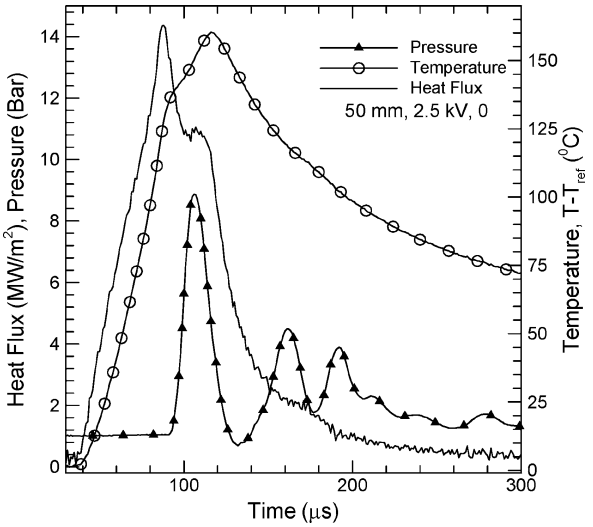

Fig. 10 Pressure, temperature, and heat flux at the stagnation location for a charging voltage of 2.5 kV (0.6 kJ) and a distance of $L = 50$ mm between plasma port and stagnation plate.

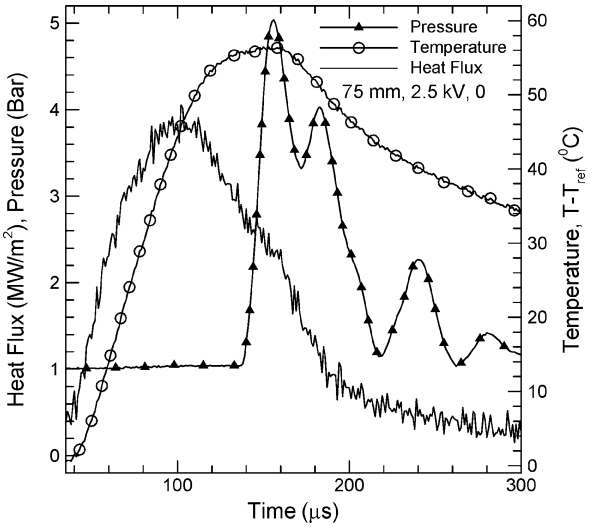

Fig. 11 Pressure, temperature, and heat flux at the stagnation location for a charging voltage of 2.5 kV (0.6 kJ) and a distance of $L = 75$ mm between plasma port and stagnation plate.

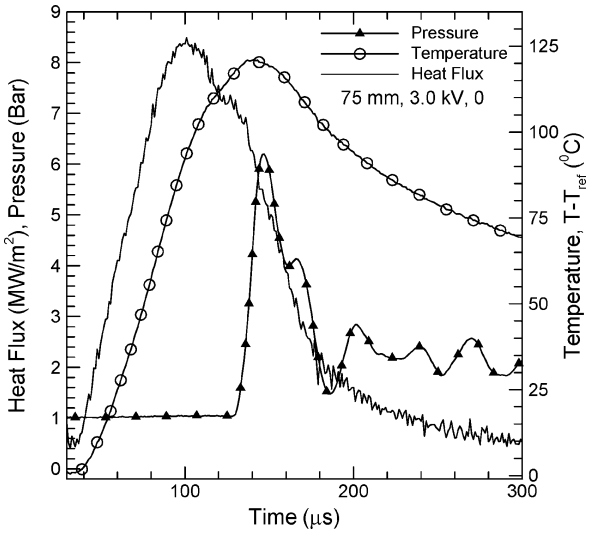

Fig. 12 Pressure, temperature, and heat flux at the stagnation location for a charging voltage of 3 kV (0.86 kJ) and a distance of $L = 75$ mm between plasma port and stagnation plate.

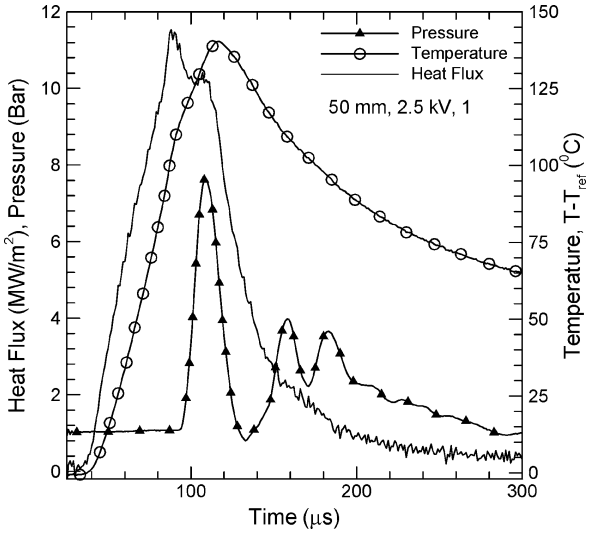

Fig. 13 Pressure, temperature, and heat flux at a position of 9.5 mm above the stagnation location (gauge 1) for a charging voltage of 2.5 kV (0.6 kJ) and a distance of $L = 50$ mm between plasma port and stagnation plate.

is important, suggesting the need for multidimensional radiation models if this problem is to be studied using computational techniques. The gasdynamic phenomena revealed by the pressure gauges are complex as discussed previously, and their general features are captured in comprehensive modeling efforts by Nusca et al.[32]

The temperature rise of the heat flux gauges is dominated by plasma emission during the time period prior to arrival of the precursor shock and shows a fairly smooth variation. After the peak of the electrical energy conversion, the plasma quickly loses its sensible energy largely by radiation, and thus the gauge temperature decreases quickly due to primarily heat conduction into the substrate and secondarily to surface emission. Furthermore, inspection of Figs. 10–13 reveals that the early portion of the plasma emission is the most intense, corresponding to the time period up to peak current flow, or peak power dissipation within the capillary. From other measurements, the plasma has traveled only about 40 mm at a time of 80 μs into the event.

Increasing the distance from 50 to 75 mm has a pronounced effect on all the peak values, demonstrating the important effect of gasdynamic expansion, directional nature of radiation, heat loss by radiation, and possibly recombination reactions among plasma species. A two-stage radiant heating effect is observed clearly in Figs. 10 and 13, whereas it is only slightly detected in Fig. 11. The first stage is caused by the strong plasma emission prior to arrival of the precursor shock. The second stage is likely caused by increased pressure and temperature near the stagnation point, as plasma accumulates and recombination reactions occur, some of which may produce emission due to electronic transitions in atomic and molecular species. Figures 10 and 13 show that small but measurable differences in pressure arrival and magnitude, as well as temperature and deduced radiant heat flux, occur between gauges located at the stagnation point and 9.5 mm above the stagnation point. The gasdynamic phenomena also show a slight phase shift in Figs. 10 and 13.

The plasma radiation is both spectral and directional and has a strong nonlinear dependence on temperature. To push the gauges to their limits and beyond, we show in Figs. 14 and 15 the results for a charging level of 4 kV and distance of 50 mm. Of the five gauges used on the stagnation plate, three were completely vaporized, a fourth was damaged, whereas the outermost gauge survived. Since the calibration was performed up to a temperature of 220°C, the results for gauges 0 and 2 are terminated near 280°C. The observed phenomena discussed previously are evident

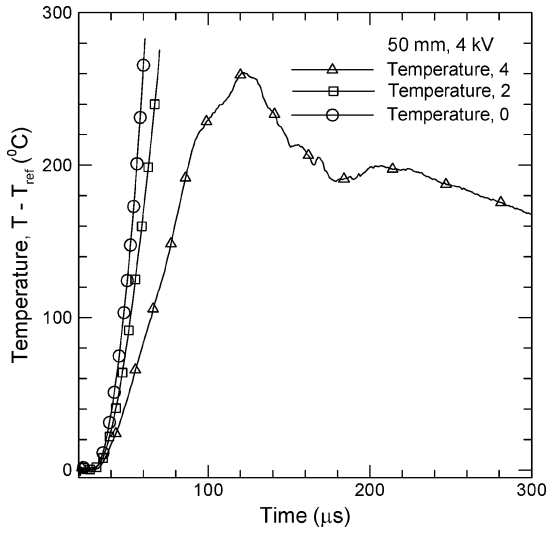

Fig. 14 Temperature of three heat flux gauges separated by 19 mm on the stagnation plate for a charging voltage of 4.0 kV (1.56 kJ) and a distance of $L = 50$ mm between plasma port and stagnation plate.

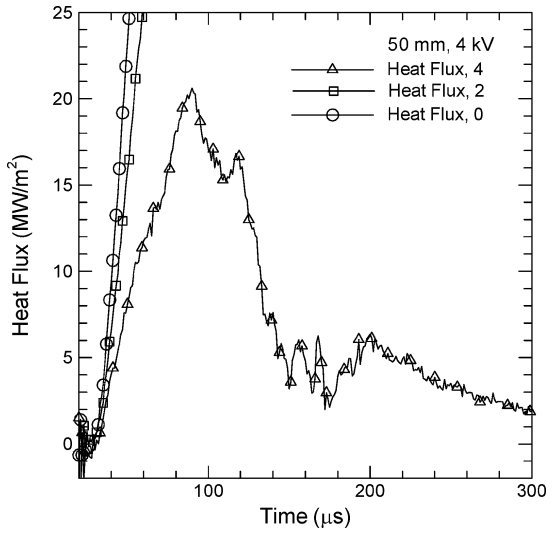

Fig. 15 Deduced absorbed radiative heat flux of three gauges separated by 19 mm on the stagnation plate for a charging voltage of 4.0 kV (1.56 kJ) and a distance of $L = 50$ mm between plasma port and stagnation plate.

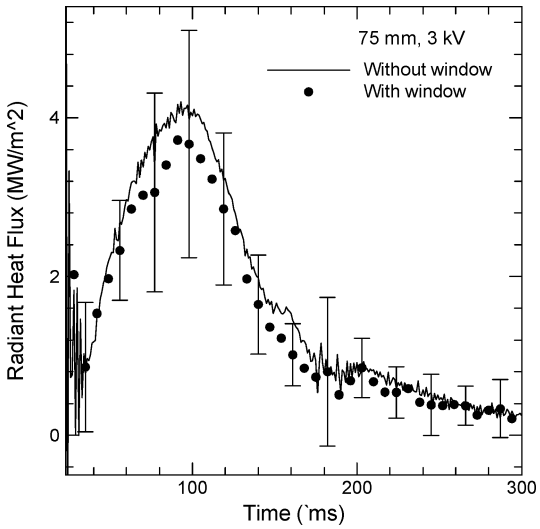

Fig. 16 Deduced radiative heat flux for gauges located below the plasma with and without the fused-silica window.

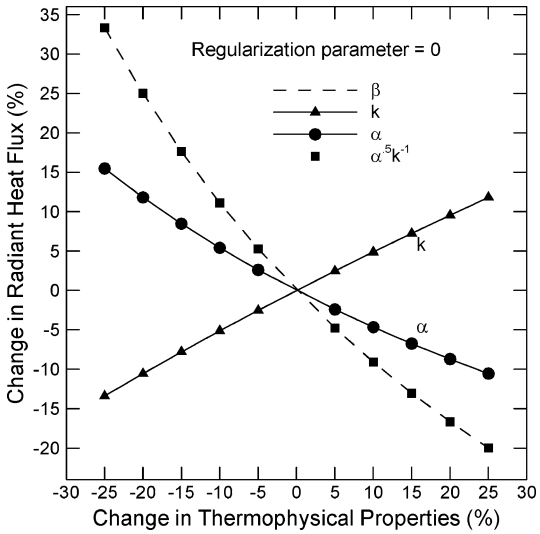

Fig. 17 Effect of uncertainty in electrical and thermal transport input data on the deduced radiative heat flux.

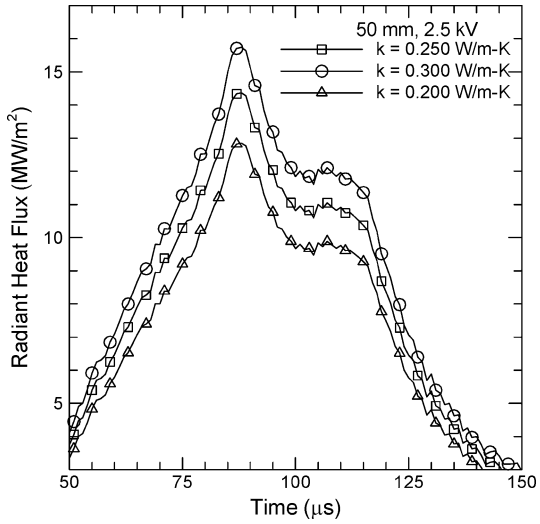

Fig. 18 Effect of uncertainty in thermal conductivity on the deduced radiative heat flux.

again, largely by gauge 4, which is located 38 mm above the stagnation point. The peak level of the radiative heat flux of gauge 4 is slightly above 20 MW/m^2, whereas much higher values would be reached at the stagnation point. Plasma emission is dominant prior to arrival of precursor shock, during which some of the oscillating gasdynamic effects can be seen in the deduced radiative heat flux; plasma emission is much lower after the electrical discharge is complete.

To assess the role of the fused-silica window and its effect on the deduced radiative heat flux, Fig. 16 shows the results with and without the fused-silica window for gauges mounted 75 mm below the plasma port. These results were obtained from averaging data from three experiments and four heat flux gauges; the effect of gauge position is not significant when mounting gauges below the plasma. Inspection of the results in Fig. 16 reveals that a reduction of only about 12% is obtained by using the fused-silica window. This reduction is quite acceptable, because the spectral transmissivity of the window ranges from about 0.92 at 200 nm to 0.94 at 700 nm (data from ESCO Products). Hence, the effect of the direction of the radiant energy emitted by the plasma on the deduced absorbed radiant flux levels is at best marginal. Furthermore, these results also suggest that the spectral range from about 200 to 2500 nm of the fused-silica window includes the dominant fraction of the radiant energy emitted by the plasma. Rovibrational transitions in the infrared wavelength range beyond 2500 nm by molecular species, such as C_xH_y, do not appear to contribute significantly to the radiative heat flux, although diode 2 did record some effects from electronic transitions in the visible wavelength range well beyond the conclusion of the electrical power conversion as mentioned earlier. Additionally, the error bars included represent a 99% confidence interval among the four gauges, which is obtained by multiplying the standard deviation by 2.565 and dividing by the square root of the degrees of freedom.

It is well known that inverse techniques are susceptible to error magnification. That is, a relatively small uncertainty in an input parameter may cause a large uncertainty in the estimated values. In the present combined experimental and numerical effort, the thermal conductivity of polyimide and the temperature coefficient contains the largest uncertainty. Other input values are the density and specific heat, but the uncertainties of these values are usually much smaller. Figure 17 shows the effects of varying the input parameter on the estimated radiative heat flux. It is observed that, over the range of change in thermophysical properties, the response is reasonably linear. Within the algorithm, the temperature coefficient β and the term $\alpha^{0.5}k^{-1}$ appear as a product, thus showing the identical results in Fig. 17. The uncertainty in the measured temperature coefficient is approximately 10%, suggesting a similar uncertainty in the estimated radiant heat flux. However, experiments will be conducted in the future to determine the thermal conductivity of the polyimide film, which may be anisotropic.

To demonstrate the temporal effect of uncertainty in the thermal conductivity and the temperature coefficient of the electrical resistivity, Figs. 18 and 19 show the results of the estimated radiative heat flux at the stagnation point for a distance of 50 mm between plasma port and stagnation plate, and a charging level of 2.5 kV. These two input parameters were changed in increments with a maximum of $\pm 20\%$ in the inverse technique. Inspection of these results shows that the trends remain the same and that peak values do not shift temporally. That is, a large uncertainty early in the event does not affect the results later in the event.

Apart from the thermophysical properties, several other sources can contribute to measurement uncertainties. One possible source of uncertainty is atmospheric attenuation of radiation for wavelengths below 300 nm; however, the potential role of atmospheric attenuation is not addressed in the present study. Another possible source of uncertainty is the vapor shield created by plasma condensation on the window, preventing radiative flux to reach the gauge.[16,33–36] In the present configuration, however, the radiative flux attains its peak before the plasma reaches the window, confining the possible vapor shield effect to the later part of the event only. The potential presence of a vapor shield requires further investigation. Experiments,

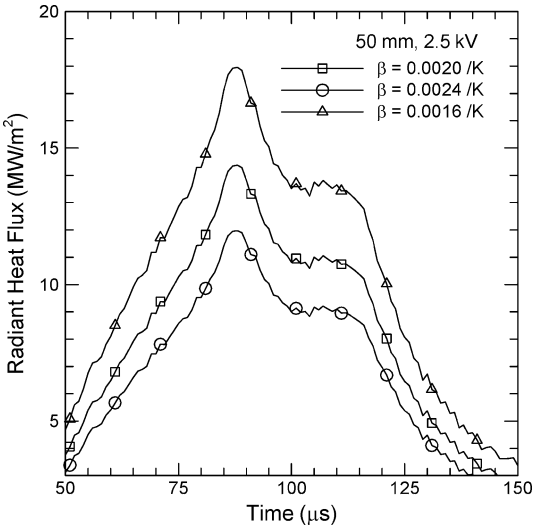

Fig. 19 Effect of uncertainty in the temperature coefficient of the electrical resistivity on the deduced radiative heat flux.

however, were conducted to identify the effect of material deposition over the sacrificial windows. Two consecutive experiments without replacing the sacrificial window showed a 7% maximum deviation in measured heat flux.

IV. Conclusions

The use of thin platinum films sputtered on a polyimide substrate has been described for deducing the transient variation of the absorbed radiative heat flux emitted from a plasma produced by a capillary discharge. The major findings from this study are as follows.

1) The radiative heat flux reached a maximum immediately after the electrical power conversion reached a maximum.

2) The spectral transmission range of the fused-silica window indicates that the major fraction of the radiative heat transfer occurred from about 170 to 2500 nm.

3) Once it arrived at the location of the heat flux sensors, the emission from the plasma was significantly reduced compared to its peak values, as a result of significant radial expansion of the plasma and rapid heat losses by radiation in all directions.

The present study deals with radiative heat transfer from a plasma produced by relatively low charging voltages. Future studies will consider other geometries, higher charging voltages, different capillary, wire, and window materials, as well as other heat transfer mechanisms.

Acknowledgments

This work was supported by the U.S. Army Research Laboratory and the U.S. Army Research Office under contracts DAAG55-98-1-0519 and DAAD19-03-1-0340 with the management of David M. Mann.

References

[1]Beyer, R. A., and Pesce-Rodriguez, R. A., "Experiments to Define Plasma-Propellant Interactions," *IEEE Transactions on Magnetics*, Vol. 39, No. 1, 2003, pp. 207–211.

[2]Fifer, R. A., Sagan, E. S., and Beyer, R. A., "Chemical Effects in Plasma Ignition," *IEEE Transactions on Magnetics*, Vol. 39, No. 1, 2003, pp. 218–222.

[3]Perelmutter, L., Sudai, M., Goldenberg, C., Kimhe, D., Zeevi, Z., Arie, S., Melnik, M., and Melnik, D., "Temperature Compensation by Controlled Ignition Power in SPETC Guns," *Proceedings of the 16th International Symposium on Ballistics*, Vol. 1, National Defense Industrial Association, Arlington, VA, 1996, pp. 145–152.

[4]Birk, A., Del Guercio, M., Kinkennon, A., Kooker, D. E., and Kaste, P., "Interrupted-Burning Tests of Plasma Ignited JA2 and M30 Grains in a Closed Chamber," *Propellants, Explosives, Pyrotechnics*, Vol. 25, No. 3, 2000, pp. 133–142.

[5]Kim, J. U., Clemens, N. T., and Varghese, P. L., "Experimental Study of the Transient Underexpanded Jet Generated by Electrothermal Capillary Plasma," *Journal of Propulsion and Power*, Vol. 18, No. 6, 2002, pp. 1153–1160.

[6]Kappen, K., and Beyer, R. A., "Progress in Understanding Plasma-Propellant Interaction," *Propellants, Explosives, Pyrotechnics*, Vol. 28, No. 1, 2003, pp. 32–36.

[7]Li, J.-Q., Litzinger, T. A., and Thynell, S. T., "Interactions of Capillary Plasma with Double-Base and Composite Propellants," *Journal of Propulsion and Power*, Vol. 20, No. 4, 2004, pp. 675–683.

[8]Li, J.-Q., Litzinger, T. A., and Thynell, S. T., "Plasma Ignition and Combustion of JA2 Propellant," *Journal of Propulsion and Power*, Vol. 21, No. 1, 2005, pp. 44–53.

[9]Williams, A. W., and White, K. J., "Plasma-Propellant Interaction Studies: Measurements of Heat Flux Produced by Hydrocarbon Ablation-Supported Plasmas," *IEEE Transactions on Magnetics*, Vol. 37, No. 1, 2001, pp. 203–206.

[10]White, K., Williams, A., and Nusca, M., "Plasma Output and Propellant Radiation Absorption Characteristics," *Proceedings of the 35th JANNAF Combustion Meeting*, Chemical Propulsion Information Agency, Publ. 680, Vol. 1, 1998, pp. 237–246.

[11]Taylor, M. J., "Measurement of the Properties of Plasma from ETC Capillary Plasma Generators," *IEEE Transactions on Magnetics*, Vol. 37, No. 1, 2001, pp. 194–198.

[12]Taylor, M. J., "Ignition of Propellant by Metallic Vapour Deposition for an ETC Gun System," *Propellants, Explosives, Pyrotechnics*, Vol. 26, No. 3, 2001, pp. 137–143.

[13]Hankins, O. E., and Mann, D., "Analyses of Molecular and Neutral Atomic Emission Spectra from an Electrochemical Launcher Plasma," *IEEE Transactions on Magnetics*, Vol. 31, No. 1, 1995, pp. 410–413.

[14]Hankins, O. E., Bourham, M. A., Earnhart, J., and Gilligan, J. G., "Visible Light Emission Measurements from a Dense Electrothermal Launcher Plasma," *IEEE Transactions on Magnetics*, Vol. 29, No. 1, 1993, pp. 1158–1161.

[15]Hankins, O. E., Bourham, M., and Mann, D., "Observations of Visible Light Emission from Interactions Between an Electrothermal Plasma and a Propellant," *IEEE Transactions on Magnetics*, Vol. 33, No. 1, 1997, pp. 295–298.

[16]Taylor, M. J., "Evidence for the Hypothesis of Ignition of Propellants by Metallic Vapour Deposition," *Propellants, Explosives, Pyrotechnics,* Vol. 27, No. 6, 2002, pp. 327–335.

[17]Proud, W. G., and Bourne, N. K., "The Electrothermal Enhancement of Propellant Burning by Plasma Injection," *Propellants, Explosives, Pyrotechnics,* Vol. 22, No. 4, 1997, pp. 212–217.

[18]Taylor, M. J., "Spectral Acquisition and Calibration Techniques for the Measurements of Radiative Flux Incident upon Propellant," *Propellants, Explosives, Pyrotechnics*, Vol. 28, No. 3, 2003, pp. 18–25.

[19]Taylor, M. J., "Direct Measurement of Radiative Flux Incident upon Propellant During Plasma Propellant Interactions," *Propellants, Explosives, Pyrotechnics*, Vol. 28, No. 3, 2003, pp. 26–31.

[20]Gruber, K., Kappen, K., Voronov, A., and Haak, H., "Radiation Absorption of Propellant Gas [in Electrothermochemical Launchers]," *IEEE Transactions on Magnetics*, Vol. 37, No. 1, 2001, pp. 161–164.

[21]Kappen, K., and Bauder, U. H., "Calculation of Plasma Radiation Transport for Description of Propellant Ignition and Simulation of Interior Ballistics in ETC Guns," *IEEE Transactions on Magnetics*, Vol. 37, No. 1, 2001, pp. 169–172.

[22]Kappen, K., and Bauder, U. H., "Simulation of Plasma Radiation in Electrothermalchemical Accelerators," *IEEE Transactions on Magnetics*, Vol. 35, No. 1, 1999, pp. 192–196.

[23]Epstein, A. H., Guenette, G. R., Norton, R. J. G., and Yuzhang, C., "High-Frequency Response Heat-Flux Gauge," *Review of Scientific Instruments*, Vol. 57, No. 4, 1986, pp. 639–649.

[24]Piccini, E., Guo, S. M., and Jones, T. V., "The Development of a New Direct-Heat-Flux Gauge for Heat-Transfer Facilities," *Measurement Science and Technology*, Vol. 11, No. 4, 2000, pp. 342–349.

[25]Buttsworth, D. R., and Jones, T. V., "Fast-Response Total Temperature Probe for Unsteady Compressible Flows," *Journal of Engineering for Gas Turbines and Power*, Vol. 120, No. 4, 1998, pp. 694–702.

[26]Walker, D. G., and Scott, E. P., "Evaluation of Estimation Methods for High Unsteady Heat Fluxes from Surface Measurements," *Journal of Thermophysics and Heat Transfer*, Vol. 12, No. 4, 1998, pp. 543–551.

[27]Cook, W. J., and Felderman, E. J., "Reduction of Data from Thin Film Heat Transfer Gages: A Concise Numerical Technique," *AIAA Journal*, Vol. 4, No. 3, 1966, pp. 561, 562.

[28]Ozisik, M. N., *Heat Conduction*, 2nd ed., Wiley, New York, 1993.

[29]Hogendoorn, C. J., de Lange, H. C., and van Steenhoven, A. A., "Design Optimization for Fast Heat-Transfer Gauges," *Measurement Science and Technology*, Vol. 9, No. 3, 1998, pp. 428–434.

[30]Kurabayashi, K., Asheghi, M., Touzelbaev, M., and Goodson, K. E., "Measurement of the Thermal Conductivity Anisotropy in Polyimide Films," *Journal of Microelectromechanical Systems*, Vol. 8, No. 2, 1999, pp. 180–191.

[31]Lide, D. R. (ed.), *CRC Handbook of Chemistry and Physics*, CRC Press, Boca Raton, FL, 1997.

[32]Nusca, M. J., McQuaid, M. J., and Anderson, W. R., "Numerical Model of the Plasma Jet Generated by an Electrothermal-Chemical Igniter," *Journal of Thermophysics and Heat Transfer*, Vol. 16, No. 1, 2002, pp. 157–160.

[33]Taylor, M. J., "Ignition of Propellant by Metallic Vapor Deposition for an ETC Gun System," *Propellants, Explosives, Pyrotechnics*, Vol. 26, No. 3, 2001, pp. 137–143.

[34]Mohanti, R. B., and Gilligan, J. G., "Time Dependent Simulation of the Plasma Discharge in an Electrothermal Launcher," *IEEE Transactions on Magnetics*, Vol. 29, No. 1, 1993, pp. 585–590.

[35]Edwards, C. M., Bourham, M. A., and Gilligan, J. G., "Experimental Studies of the Plasma-Propellant Interface for Electrothermal-Chemical Launchers," *IEEE Transactions on Magnetics*, Vol. 31, No. 1, 1995, pp. 404–409.

[36]Bourham, M. A., and Gilligan, J. G., "Analysis of Solid Propellant Combustion Behavior Under Electrothermal Plasma Injection for ETC Launchers," *IEEE Transactions on Magnetics*, Vol. 33, No. 1, 1997, pp. 278–283.